International Journal of Heat and Mass Transfer 51 (2008) 5204–5208

Contents lists available at ScienceDirect

International Journal of Heat and Mass Transfer

journal homepage: www.elsevier.com/locate/ijhmt

To the theory of underwater ice evolution, or nonlinear dynamics of "false bottoms"

D.V. Alexandrov *, I.G. Nizovtseva

Urals State University, Department of Mathematical Physics, Lenin Avenue 51, Ekaterinburg 620083, Russian Federation

ARTICLE INFO

Article history:
Received 24 September 2007
Received in revised form 13 November 2007
Available online 28 May 2008

Keywords:
Sea ice
Mushy layer
Heat fluxes
Melt pond
False bottom

ABSTRACT

We present a mathematical model describing evolution of false bottoms often met between an under-ice melt pond and the underlying ocean during summer. The model treats a false bottom as the region of mixed phase (mushy layer) whose coordinates depend on time and determine the phase transition area. As the heat and the salt fluxes in the ocean are strongly influenced by turbulence and the ice meltwater accumulating underneath the ice cover is practically fresh, we use modified boundary conditions for heat and mass fluxes at the interfaces of phase transition. Explicit analytical solutions (thickness of false bottom and growth rates of its boundaries, temperature and salinity distributions, solid phase fraction and ocean-to-ice heat flux) of the nonlinear model under consideration are found. Model predictions are in good agreement with existing experimental data and physical concepts of phenomena under study.

1. Introduction

During the summer, when the air temperature is above 0 °C the sea ice – atmosphere interface undergoes ablation to occur. A considerable fraction of meltwater gathers in surface puddles thereby reducing the surface albedo. This meltwater can percolate into the ice matrix, leading to a strong reduction in the surface salinities. Untersteiner [1] showed that the meltwater flux into the ice reduces salinities at the top of the ice column to values close to zero. As a result of these processes, low-salinity meltwater comes into contact with seawater, each at or close to their respective freezing points. This meltwater can be retained under thin ice in bottom depressions, leading to fresh water lenses or forming what Hanson calls "under-ice melt ponds" [2]. Martin and Kauffman demonstrated in their laboratory experiments that freezing of under-ice melt ponds can be explained by double-diffusion at the interface between freshwater and seawater [3]. Initially, ice platelet crystals would form in the contact zone and grow to centimeter or decimeter size if an attachment prevented their removal from the halocline. Subsequently, more solid ice cover would form along the entire freshwater – seawater interface, stabilized by a mesh of crystals and other anchor processes. This underwater ice is called false bottoms [2–6]. When this underwater ice sheet forms, it migrates upwards due to bottom ablation [2,3] (for example, the Arctic Ice Dynamics Joint Experiment (AIDJEX) demonstrated some rapid upward migration of the false bottoms with relation to ablation under nearby thick ice). The field experiment Surface Heat Budget of the Arctic Ocean (SHEBA) showed that approximately 15% of a total of more than 100 mass-balance gauges developed false bottoms during the ablation season [6,7]. It has been found experimentally that under-floe melt ponds and false bottoms covered half of the flow bottom of the drifting station "Charlie" [2]. It is important to keep in mind that the formation of false bottoms is the only process by which significant amounts of new ice can be formed during the summertime. Nansen from his observations in the Beaufort Sea noted that the heat transfer from the trapped fresh water, with a temperature of 0 °C, to the arctic sea water, with a temperature of −1.6 °C, is the only source of ice accretion during the polar summer [8]. An additional point to emphasize is that false bottoms play an important role as reservoirs of meteoric water (snow meltwater). They are important in the transfer of pollutants from the atmosphere into the ice pack [9]. Taking into account all things considered, we present a theory of false bottom migration on the basis of macroscopic heat and mass transfer equations and boundary conditions when the phase transition occurs in a mixed layer (mushy region) and the heat and mass fluxes in the ocean are influenced by turbulence.

2. Model of false bottom evolution

Let us now consider the process when a false bottom directionally freezes upwards. We describe a system once a thin veneer of young ice representing a false bottom has been formed (the initial formation of false bottoms usually took only a couple of hours in natural conditions [10]). A schematic diagram of the process is plotted in Fig. 1 (here z is the spatial coordinate, $a(t)$ and $b(t)$ are the fresh water – false bottom and false bottom – sea water phase transition interfaces, respectively, t is the time). The regions $a(t) < z < 0, z < b(t)$ and $b(t) < z < a(t)$ are, respectively, filled

* Corresponding author. Tel.: +7 343 3 507541; fax: +7 343 3 507401.
E-mail address: Dmitri.Alexandrov@usu.ru (D.V. Alexandrov).

0017-9310/$ - see front matter © 2008 Elsevier Ltd. All rights reserved.
doi:10.1016/j.ijheatmasstransfer.2007.11.061

Nomenclature

a	fresh water – false bottom boundary
b	false bottom – sea water boundary
c_w	specific heat of water
D	molecular diffusivity of salt in sea water
k_i	thermal conductivity of ice
k_w	thermal conductivity of water
L_V	latent heat
m	liquidus slope
S_m	salinity
S_∞	salinity far from phase transition boundaries in the ocean
t	time
T_∞	temperature far from phase transition boundaries in the ocean
u	friction velocity
z	spatial coordinate

Greek symbols

α_h	turbulent coefficient for heat
α_s	turbulent coefficient for salt
ρ_w	density of water
φ	solid phase fraction

Subscripts

a and b	point at the physical parameters of boundaries $a(t)$ and $b(t)$.

with the fresh water, the sea water and the false bottom consisting of a mixed (liquid and solid phases) zone [3,5]. We shall treat this zone as a quasi-equilibrium mushy layer [11,12]. Since a relaxation time of the temperature field is far less than characteristic times of the process, the temperature field in the mushy layer (false bottom) will be considered as a linear function of the spatial coordinate

$$T_m(z,t) = \frac{T_a(t)(z-b(t)) + T_b(t)(a(t)-z)}{a(t)-b(t)}, \quad b(t) < z < a(t), \tag{1}$$

where T_a and T_b stand for the temperatures at the phase transition boundaries a and b. The linear form (1) of the temperature field is confirmed by laboratory experiments [3]. Physically this means that the temperature field and the solid fraction $\varphi(z,t)$ within the false bottom undergo only insignificant oscillations with time (φ is also with z). Theoretically this conclusion was demonstrated by Alexandrov and Malygin [13] and by Alexandrov et al. [14] for solidification of leads. Taking into account that the salinity field $(S_m(z,t))$ in the mush is a nearly linear function of z (see among others, [3]), we use the Scheil formula [15]

$$\frac{\partial}{\partial t}((1-\varphi)S_m) = 0, \quad b(t) < z < a(t). \tag{2}$$

Eq. (2) implies that all salt is displaced by ice into the liquid matrix of the system. We shall consider that the mushy layer (false bottom) is in thermodynamic equilibrium. Therefore, the temperature and salinity distributions are related by the liquidus equation

$$T_m(z,t) = -mS_m(z,t), \quad b(t) < z < a(t), \tag{3}$$

where m is the liquidus slope. The linear form of Eqs. (1) and (3) agrees closely with the laboratory experiments [3] where nearly linear functions T_m and S_m with respect of z have been observed.

Laboratory experiments [3] show that heat and the salt fluxes at the phase transition boundary $z = a(t)$ determined from the fresh water side are far less than their analogs determined from the mushy layer side. This being the case, the heat and mass balance boundary conditions can be written in the form

$$L_V\varphi_a\frac{da}{dt} = (k_i\varphi_a + k_w(1-\varphi_a))\frac{\partial T_m}{\partial z}, \tag{4}$$

$$S_a\frac{da}{dt} = -D\frac{\partial S_m}{\partial z}, \tag{5}$$

where L_V is the latent heat parameter, D is the diffusion coefficient, k is the thermal conductivity, the subscripts i and w refer to ice and water, respectively. Eq. (5) indicates that the rate of salt diffusion must be sufficient to keep up with the rate of boundary $a(t)$ (this model assumption is backed by the laboratory experiments [3] demonstrating that the salinity gradient is practically negligible in the fresh water region at $z \geqslant a(t)$).

As the rate of motion of the phase transition boundary $z = b(t)$ undoubtedly depends on the turbulent motion in the ocean, let us write down the boundary conditions as follows [10,16,17]

$$L_V\varphi_b\frac{db}{dt} = (k_i\varphi_b + k_w(1-\varphi_b))\frac{\partial T_m}{\partial z} + \alpha_h\rho_w c_w u(T_\infty - T_b), \tag{6}$$

$$S_b\varphi_b\frac{db}{dt} = \alpha_s u(S_\infty - S_b), \tag{7}$$

where T_∞ and S_∞ are the far-field properties of the salt water, u is the friction velocity, ρ_w and c_w are the density and the specific heat of water, α_h and α_s are the turbulent transfer coefficients for heat and salt respectively. The ratio of exchange coefficients α_h/α_s depends on the molecular diffusivities for heat (κ) and salt (D) at that $\alpha_h/\alpha_s = (\kappa/D)^n$ [17] with $2/3 < n < 4/5$ [18,19]. We put $35 \leqslant \alpha_h/\alpha_s \leqslant 70$ after Notz et al. [10]. The aforementioned model (1)–(7) represents a nonlinear set of equations and boundary conditions imposed at moving phase transition interfaces. This

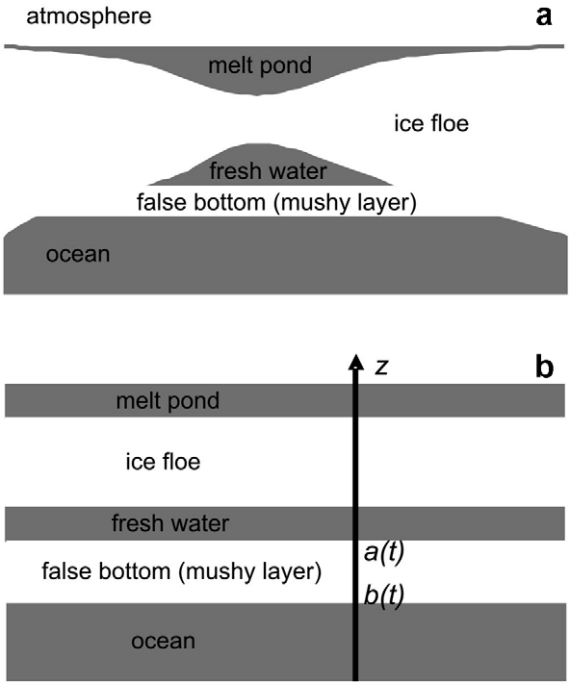

Fig. 1. (a) A sketch of an under-ice melt pond [3]. (b) A schematic diagram of the process.

model describes nonstationary freezing in the presence of a mushy layer, playing the role of a false bottom, with heat and salt fluxes at the lower boundary influenced by turbulence. How to construct exact analytical solutions of the above-mentioned model is discussed below.

3. Exact analytical solutions

Integrating Eq. (2), we find the solid phase fraction in the mushy layer

$$\varphi(z,t) = 1 - \frac{(1-\varphi_b)T_b}{T_m(z,t)}, \tag{8}$$

where $T_m(z,t)$ is determined by expression (1). Combining the boundary conditions (4), (5) and taking into account Eq. (3), we get the solid phase fraction at the upper phase transition interface

$$\varphi_a(t) = \frac{KT_a(t)}{(K-1)T_a(t) - T_p}, \quad K = \frac{k_w}{k_i}, \quad T_p = \frac{DL_V}{k_i}. \tag{9}$$

Now substituting $\varphi_a(t)$ from expression (9) into expression (8) at $z = a(t)$, we obtain temperature T_b at the lower boundary in terms of temperature T_a at the upper boundary

$$T_b(T_a(t)) = \frac{T_a^2(t) + T_a(t)T_p}{(\varphi_b - 1)((K-1)T_a(t) - T_p)}. \tag{10}$$

As the temperature and salinity fluxes are proportional in accordance with Eqs. (1) and (3) we can find a set of equations connecting the mushy layer (false bottom) thickness $h(t) = a(t) - b(t)$ and the phase transition temperature $T_a(t)$. With this aim in mind we equate derivatives db/dt from Eqs. (6) and (7) and subtract derivatives in the left-hand sides of Eqs. (4) and (7). As a result, we have

$$a(t) - b(t) = Q_1(T_a(t), t), \tag{11}$$

$$\frac{d(a(t)-b(t))}{dt} = \frac{Q_2(T_a(t))}{a-b} + Q_3(T_a(t), t), \tag{12}$$

where

$$Q_1(T_a(t),t) = -\frac{(k_i\varphi_b + k_w(1-\varphi_b))(T_a - T_b)T_b}{\alpha_s u L_V(T_b + mS_\infty) + \alpha_h \rho_w c_w u(T_\infty - T_b)T_b},$$

$$Q_2(T_a(t)) = \frac{(k_i\varphi_a + k_w(1-\varphi_a))(T_a - T_b)}{L_V\varphi_a},$$

$$Q_3(T_a(t),t) = \frac{\alpha_s u(T_b + mS_\infty)}{T_b\varphi_b}.$$

Here we bear in mind that the arguments of functions Q_1, Q_2 and Q_3 may be dependent on time in an explicit form (not only by means of dependence $T_a(t)$) in the case that u, T_∞ or S_∞ are time-dependent too.

Let us now consider the special case that all values u, T_∞ and S_∞ are constants (or all of them are averaged over their variations in time and changed by constants). Then Q_1 and Q_3 as well as Q_2 depend on t only as composed functions of $T_a(t)$. If this is really the case, substitution $a(t) - b(t)$ from (11) into (12) gives an explicit function $t(T_a)$ of the form

$$t(T_a) = \int_{T_{a0}}^{T_a} F(T_a)dT_a, \quad F(T_a) = \frac{dQ_1(T_a)}{dT_a}\frac{Q_1(T_a)}{Q_2(T_a) + Q_1(T_a)Q_3(T_a)}. \tag{13}$$

The initial temperature T_{a0} (determined at $t = 0$) can be found from the algebraic Eq. (11) on condition that the initial coordinates $a(0)$ and $b(0)$ are known. Once integral in the right-hand side of (13) has been calculated, the inverse function $T_a(t)$ can readily be obtained.

In the general case when one of the values u, T_∞ or S_∞ becomes dependent on time, we can get the initial-value problem (Cauchy problem) for $T_a(t)$; if so, substitution $a(t) - b(t)$ from (11) into (12) gives

$$\frac{dT_a(t)}{dt} = f(T_a, t), \quad T_a(0) = T_{a0}, \tag{14}$$

where $f(T_a, t)$ is known function. For the sake of simplicity, we will not write out this elementary but exceedingly lengthy dependence. The initial point T_{a0} is determined, as before, by Eq. (11).

We are now in position to describe the laws of motion of boundaries $a(t)$ and $b(t)$; to accomplish this, let us integrate expression (7) and arrive at the law for lower boundary

$$b(t) = b(0) - \int_0^t \frac{\alpha_s u(T_b(T_a) + mS_\infty)}{T_b(T_a)\varphi_b}\,dt, \tag{15}$$

where $T_b(T_a)$ and $T_a(t)$ are determined by expressions (10), (13) or (14). The law of upper boundary follows from Eq. (11) and has the form

$$a(t) = b(t) + Q_1(T_a(t), t). \tag{16}$$

4. Model predictions for field experiments

Let us now compare model predictions and experimental data on false bottom evolution taken from the AIDJEX and the SHEBA field experiments (see, among others, [20,21]). Since the solid fraction φ_b is in close proximity to unity, we choose $\varphi_b = 0.99$. Fig. 2 demonstrates the bottom elevation change during AIDJEX calculated on the basis of expression (15) for different friction velocities ($b_1(t) = b(t) - b(0)$) and Fig. 3 shows time oscillations of the solid fraction φ_a and the heat flux $J = \alpha_h\rho_w c_w u(T_\infty - T_b)$ that goes from the false bottom – ocean interface to the ocean (this direction corresponds to negative values of J). The far-field temperature, T_∞, and salinity, S_∞, as well as the friction velocity, u, can vary with time in natural conditions. Figs. 4 and 5 demonstrate such variations measured during the 1998 SHEBA campaign in accordance with ref. [10]. Using these experimental data as the base let us take a brief look at time-to-time variation of the false bottom thickness $h(t) = a(t) - b(t)$. Fig. 5 demonstrates this function calculated on the basis of expressions (14)–(16). It is readily seen that the essentially increasing function $h(t)$ becomes decreasing after day 207. The reason is that the storm came through, which substantially increased function $u(t)$ (see Fig. 5 and Ref. [10]). As a result, the salt flux from the ocean to the ice increases, and in its turn a rapid ablation of the false bottom occurs. An increase of the brine salinity reduces the phase transition temperature $T_b = -mS_b$ which becomes less than the ocean temperature T_∞. By this is meant that the tem-

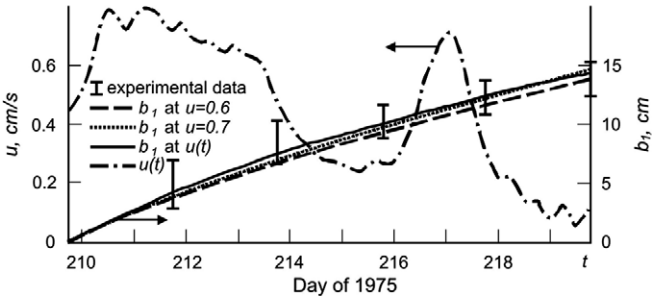

Fig. 2. Friction velocity during AIDJEX in accordance with Rossby-number similarity theory [10] (axis to the left). Experimental data in accordance with the AIDJEX field campaign and theoretical predictions (axis to the right). Two curves based on fixed values of u are calculated from expression (13) and one curve based on time oscillations of $u(t)$ is calculated from expression (14). Thermophysical parameters used in calculations [3,10]: $\alpha_h = 0.0095, \alpha_h/\alpha_s = 35, k_w = 5.86\cdot10^{-3}$ J/(cm c °C), $k_i = 22.19\cdot10^{-3}$ J/(cm c °C), $c_w = 4.187$ J/(g °C), $\rho_w = 1$ g/cm^3, $L_V = 308.16$ J/cm^3, $a(0) - b(0) = 2.5$ cm, $T_\infty = -1.5$ °C, $m = 5.3\cdot10^{-2}$ °C psu^{-1}, $S_\infty = 29.8$ psu.

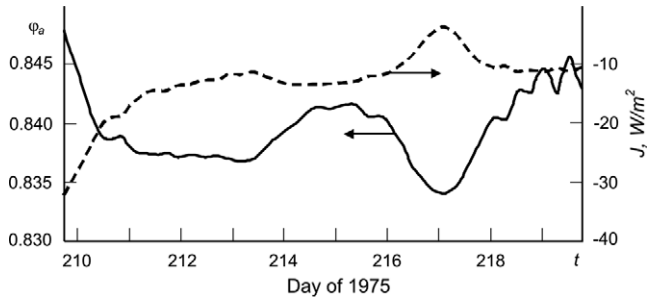

Fig. 3. The solid fraction at the fresh water – false bottom interface and the heat flux at the sea water – false bottom interface as the functions of time. These dependences are plotted in accordance with function $u(t)$ shown in Fig. 2.

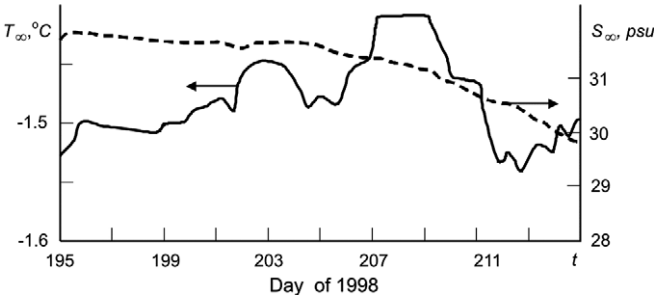

Fig. 4. Far-field temperature and salinity from SHEBA data.

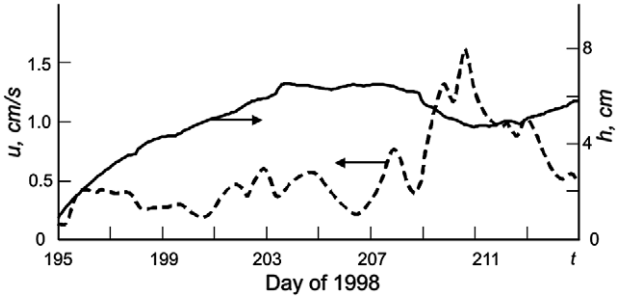

Fig. 5. Friction velocity from SHEBA data and calculated evolution of the thickness of a false bottom (mushy layer), $a(0) - b(0) = 1$ cm.

perature difference $\Delta T = T_\infty - T_b$ becomes negative and the heat flux J changes its sign. In other words, the ocean–ice heat flux in this case is directed toward the ice. Such a behavior is demonstrated in Figs. 6 and 7 where all functions are shown in accordance with the theory under consideration.

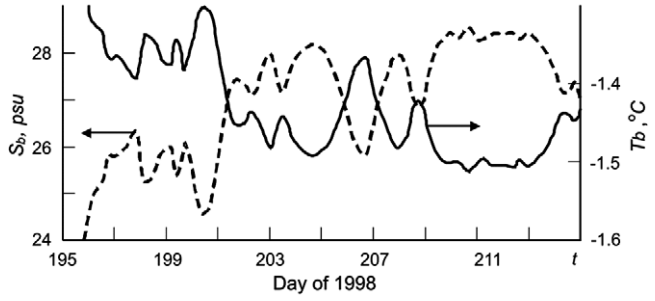

Fig. 6. Salinity and temperature oscillations predicted on the basis of our theory and SHEBA data.

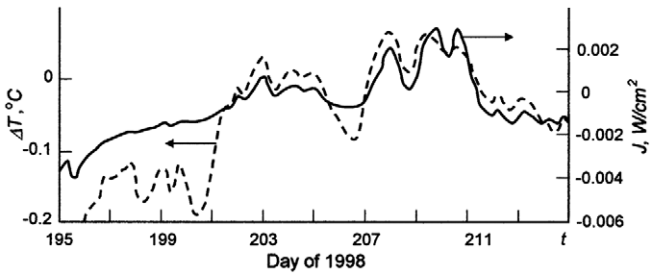

Fig. 7. ΔT and heat flux oscillations predicted on the basis of our theory and SHEBA data.

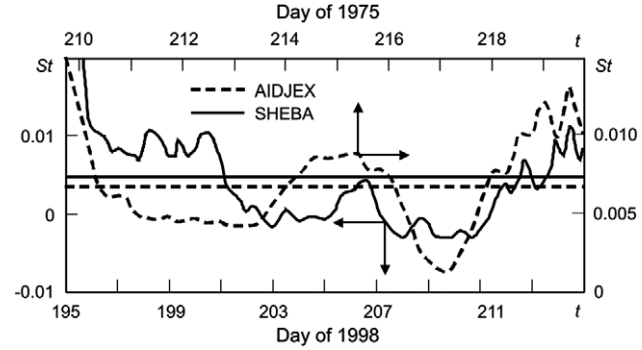

Fig. 8. Current and average heat transfer coefficients (Stanton numbers) calculated on the basis of AIDJEX (in the case of $u(t)$) and SHEBA data. Horizontal lines show corresponding average values, $\langle \mathrm{St} \rangle = 0.0067$ for AIDJEX and $\langle \mathrm{St} \rangle = 0.0047$ for SHEBA data.

We now turn our attention to the question of current fluctuations in a Stanton number

$$\mathrm{St} = -\alpha_h \frac{T_\infty - T_b}{T_\infty + mS_\infty}$$

shown in Fig. 8. A common way of treating ocean heat flux in theoretical and numerical models is to express the heat flux in terms of the heat exchange coefficient (Stanton number), relating the aggregate scale heat flux to ice interface friction velocity and elevation of mixed layer temperature above freezing [10]. Results from several studies have shown the Stanton number to be relatively uniform [22]. Its average values $\langle \mathrm{St} \rangle$ close to 0.0055 used in Ref. [10] for finding the turbulent transfer coefficients.

5. Concluding remarks

In this paper, we have focused attention on the mathematical model of false bottoms that play an important role in the energy balance of Arctic sea ice. They frequently form at the interface between fresh and salt water bordering under-ice concavities in summer. During periods of the thickening of false bottoms there is a significant heat flux into the mixed layer of order 10 W/m^2 [10]. For example, the model under consideration predicts that the ice–ocean heat flux can be directed upward or downward at different times, with an average value of -12.9 W/m^2 for AIDJEX and -5.6 W/m^2 for SHEBA data (the reason of upward direction is connected with abrupt jumps of the friction velocity). This flux is comparable to other heat fluxes such as solar radiation divergence and the upward ocean heat flux from depth. Taking into consideration that under-ice melt pond formation might be a widespread phenomenon in the Arctic [23], an important role of model predictions

becomes clear to learn more about nonlinear dynamics of the Arctic Seas.

Acknowledgements

This work was made possible in part due to the financial support of Grants Nos. 08-01-00298, 07-03-96069 Ural, 07-01-96091 Ural (Russian Foundation for Basic Research) and MD-4563.2008.2 (President Grant).

References

[1] N. Untersteiner, Natural desalinisation and equilibrium salinity profile of perennial sea ice, J. Geophys. Res. 73 (4) (1968) 1251–1257.
[2] A.M. Hanson, Studies of the mass budget of Arctic pack-ice floes, J. Glaciol. 5 (1965) 701–709.
[3] S. Martin, P. Kauffman, The evolution of under-ice melt ponds, or double diffusion at the freezing point, J. Fluid Mech. 64 (3) (1974) 507–527.
[4] N.V. Cherepanov, I.L. Nazintsev, K.P. Tyshko, Contact supercooling of water layers and bottom ice formation in the sea (in Russian), in: V.V. Bogordskii, V.P. Gavrilo (Eds.), Electro Physical and Physical–Mechanical Properties of Ice, Gidrometeoizdat, St. Petersburg, Russia, 1989, pp. 124–134.
[5] H. Eicken, Structure of under-ice melt ponds in the central Arctic and their effect on the sea-ice cover, Limnol. Oceanogr. 39 (3) (1994) 682–694.
[6] H. Eicken, H.R. Krouse, D. Kadko, D.K. Perovich, Tracer studies of pathways and rates of meltwater transport through Arctic summer sea ice, J. Geophys. Res. 107 (C10) (2002) 8046.
[7] D.K. Perovich, T.C. Grenfell, J.A. Richter-Menge, B. Light, W.B. Tucker III, H. Eicken, Thin and thinner: ice mass balance measurements during SHEBA, J. Geophys. Res. 108 (C3) (2003) 8050.
[8] F. Nansen, Farthest North, Constable, Westminster, England, 1897.
[9] R. Gradinger, Occurrence of an algal bloom under Arctic pack ice, Mar. Ecol. Prog. Ser. 131 (1996) 301–305.
[10] D. Notz, M.G. McPhee, M.G. Worster, G.A. Maykut, K.H. Schlünzen, H. Eicken, J. Geophys. Res. 108 (C7) (2003) 3223.
[11] Yu.A. Buyevich, D.V. Alexandrov, V.V. Mansurov, Macrokinetics of Crystallization, Begell House, New York, Wallingford, 2001.
[12] R.N. Hills, D.E. Loper, P.H. Roberts, A thermodynamically consistent model of a mushy zone, Q. J. Appl. Math. 36 (1983) 505–539.
[13] D.V. Alexandrov, A.P. Malygin, Analytical description of seawater crystallization in ice fissures and their influence on heat exchange between the ocean and the atmosphere, Dokl. Earth Sci. 411A (9) (2006) 1407–1411.
[14] D.V. Alexandrov, A.P. Malygin, I.V. Alexandrova, Solidification of leads: approximate solutions of non-linear problem, Ann. Glaciol. 44 (2006) 118–122.
[15] E. Scheil, Bemerkungen zur schichtkiistallbildung, Zeitschrift Fur Metallkd. 34 (1942) 70–72.
[16] M.G. McPhee, The upper ocean, in: N. Untersteiner (Ed.), The Geophysics of Sea Ice, Plenum, New York, 1986, pp. 133–141.
[17] M.G. McPhee, G.A. Maykut, J.H. Morison, Dynamics and thermodynamics of the ice/upper ocean system in the marginal ice zone of the Greenland sea, J. Geophys. Res. 92 (C7) (1987) 7017.
[18] P.R. Owen, W.R. Thomson, Heat transfer across rough surfaces, J. Fluid Mech. 15 (1963) 321.
[19] A.M. Yaglom, B.A. Kader, Heat and mass transfer between a rough wall and turbulent flow at high Reynolds and Peclet numbers, J. Fluid Mech. 62 (1974) 601.
[20] R.S. Pritchard, Sea ice processes and models, University of Washington Press, Seattle, Washington, 1980.
[21] M.G. McPhee, Turbulent stress at the ice/ocean interface and bottom surface hydraulic roughness during the SHEBA drift, J. Geophys. Res. 107 (C10) (2002) 8037.
[22] M.G. McPhee, C. Kottmeier, J.H. Morison, Ocean heat flux in the central weddell sea in winter, J. Phys. Oceanogr. 29 (1999) 1166–1179.
[23] P. Wadhams, The underside of Arctic sea ice imaged by sidescan sonar, Nature 333 (1988) 161–164.